Proceedings of the 7th International Symposium on Cavitation
CAV2009 – Paper No. 38
August 16-22, 2009, Ann Arbor, Michigan, USA

PIV-LIF DETERMINATION OF MEAN VELOCITY FIELD AND REYNOLDS STRESS TENSOR IN A CAVITATING MIXING LAYER

Vincent Aeschlimann
L.E.G.I – G-INP
BP 53 – 38041 Grenoble Cedex 9, France
Vincent.Aeschlimann@legi.grenoble-inp.fr

Stéphane Barre
L.E.G.I – G-INP - CNRS
BP 53 – 38041 Grenoble Cedex 9, France
Stephane.Barre@legi.grenoble-inp.fr

Key Words: *Cavitation; shear layer; experimental; P.I.V.-L.I.F; self similarity; Reynolds tensor.*

ABSTRACT

The purpose of this experimental study was to analyze a 2D cavitating shear layer. The global aim of this work was a better understanding and modeling of cavitation phenomena from a 2D turbulent shear flow to rocket engine turbopomp inducers.

This 2D mixing layer flow provided us a well documented test case to be used for comparison between the behavior with and without cavitation. Similarities and differences led to characterize effects of the cavitation on the flow dynamic.

The run fluid was liquid water. The experimental facility allowed us to set two distinct configurations with different cavitation levels:
- CDM: a mixing layer flow (U_1 = 15.8 m/s for the high speed side and U_2= 3.5 m/s for the low speed side)
- MD: a downward facing step flow (U_1 = 13.5 m/s and U_2 = 0 m/s).

The development of Kelvin-Helmholtz instabilities was observed at the interface. Vaporizations and implosions of cavitating structures inside the vortices were also observed.

PIV-LIF(Particle Image Velocimetry – Laser Induced Fluorescence) system was used to measure the velocity of the liquid phase. Instantaneous velocity fields were measured in the whole flow.

The Self similarity of the flow was characterized by the dimensionless analysis of the mean and fluctuating velocity fields. Parameters that characterized the flow dynamic were studied and quantified: Vorticity thickness, growth rate and Reynolds tensor components. Turbulent kinetic energy and the anisotropy tensor components were also analyzed and estimated.

General behaviors of the two configurations have been observed:
- In the CDM case the mixing area developed along the x-axis a turbulent shear area, growing linearly, showing a constant growth rate over the studied cavitation parameter range.
- The MD case was more complex, presenting a flow separation with a large recirculating area and a quite large positive pressure gradient. The reattachment point moved depending on the cavitation level. The recirculating area seemed to have an unsteady behavior and was certainly pulsing and shedding vortices downstream.

Successive vaporizations and condensations of the fluid particles inside the turbulent area have generated additional velocity fluctuations due to the strong density changes associated with the vaporization and condensation processes. However, the mean spatial development of the mixing area was only barely affected over the studied cavitation number range.

The main results of this study clearly showed that the turbulence-cavitation relationship inside a mixing layer is not only driven by a simple change of compressibility properties of the fluid in the turbulent field due to the presence of a two-phase flow.

INTRODUCTION

Background

This work follows previous experimental and numerical studies carried out by the Turbomachinery and Cavitation team of LEGI (Grenoble, France). The purpose was a better understanding and modeling of cavitation phenomenon [1] [2] [3].

The studies were led in collaboration with the French Space Agency (CNES) and the rocket engine division of Snecma. The global aims were the analyses of cavitating flows

in the rocket engine turbopomp inducers, where the run fluids are cryogenic fluids, liquid hydrogen (LH2) and liquid oxygen (LOx).

In this context, experimental and numerical studies have been performed in the laboratory, with cold water and refrigerant R114 on venturi geometries [1-6]. Those previous studies provided a good understanding of the dynamic behavior of an attached cavitating sheet on the wall. The oscillating frequency of the vapor sheet was analyzed, the "break-of cycle" was characterized. Velocity measurements highlighted the re-entrant jet dynamic. Several phenomena were suspected to influence the cavitation development: Wall effect, flow separation, shear stress, turbulence ratio, water quality… The flow complexity prevented us from telling apart the influence of each parameters on cavitation production. That conclusion led us to carry on experimental study on a fundamental case: a 2D mixing layer. This particular type of flow has been chosen because of the high number of results present in the literature. The parameters characterizing the self-similarity properties of the flow are well known whether compressible or not, whether involved liquid or gas. Those parameters are often based on inlet conditions and liquid properties. A lack of knowledge remains concerning behavior of two phase flows and especially cavitating flows where no gas is present at the inlet.

The present study is carried out with water in a 2D shear layer test bed in order to avoid wall effect. The objective is to obtain data and information concerning the behavior of the flow under different cavitation levels. This reference test provides us a well documented test case to be used for numerical simulation validation.

Cavitating shear layer

A shear layer is characterized by a discontinuity between two flows. In the present study, the development of a velocity gradient was observed. The time averaged velocity profiles are illustrated in Fig.1. Kelvin-Helmholtz instabilities developed at the interface and became eddies along the x-axis. The pressure was lower at the eddies center than in the external layers; this was where the liquid started to evaporate first. The Fig.2 is a instantaneous picture (shutter time = 20µs) of the cavitating shear flow, it shows cavitating eddies in the shear layer: There is three eddies that are clearly identified (the vapor is dark and liquid is white).

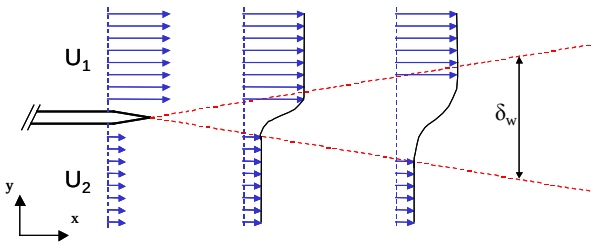

Figure 1. Averaged velocity profiles in the shear layer

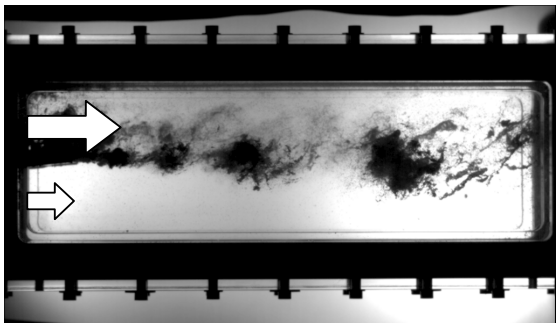

Figure 2. Instantaneous picture of the cavitating shear layer (shutter time =20µs)

A shear layer can be defined by its growth rate δ_w' which remains constant along the x-axis when the flow is self similar:

$$\delta_w' = \frac{d\delta_w}{dx}$$

where δ_w is the vorticity thickness:

$$\delta_w = \frac{U_1 - U_2}{\left.\frac{dU}{dy}\right|_{max}} = \frac{\Delta U}{\left.\frac{dU}{dy}\right|_{max}}$$

Two different behaviors occur depending on the properties of the fluid. One case is incompressible. In this case, when ΔU increases the growth rate increases too. At the opposite, in the compressible case the scaling parameter is the convective Mach number of the large eddies as defined in Papamoschou et al.[7]. When M_c increases, δ_ω' decreases. This phenomenon is called the net effect of compressibility. It can be quantified by the convective Mach number M_c which depends on the velocity difference and the speed of sound of each external flow:

$$M_c = \frac{U_1 - U_2}{(a_1 + a_2)}$$

Where a_1 and a_2 are the speed of sound for the two external flows: $a_1 = a_2 \approx 1500$ m/s in liquid water.

When M_c is lower than 0.5 the flow behaves as an incompressible one [7-8].

One of the objectives of the present study was to analyze the behavior of a two-phase flow mixing layer. The incoming flows were liquid cold water ones and the vapor appeared inside the eddies in the mixing area due to sheared cavitation. Such shear layer cannot be compared to the one obtained in gas supersonic flows as described in [7] because of the cavitation phenomenon. In our case, the convective Mach number was 0.006 which would mean the flow could be approximate to an incompressible one whereas the local Mach number inside the two-phase sheared zone in the flow was about 5. The main interest for studying such flows comes from the original configuration of two subsonic flows creating a supersonic shear layer in the two-phase mixing zone only.

METHODS

Experimental apparatus

Experiments were conducted in CREMHyG, hydraulic research center of Grenoble, in a shear layer test bed. The rectangular test section was 300 mm long and had a cross-section that expands from 80 by 80 mm at the inlet to 80 by 88.8 mm at the outlet. The studied shear layer was 2D, the inlet section was divided in two halves. The splitting plate was 6 mm thick and ends by a rounded edge of 0.2 mm diameter. Liquid water was used as the test fluid for this experiment.

The test bed was set in a hydraulic closed-circuit including a regulated water pump and a free surface tank. The pressure was decreased in the system by a vacuum pump located in the tank. The operating point was characterized by the reference cavitation number σ_{ref} defined in the inlet reference section:

$$\sigma_{ref} = \frac{P_2 - P_v}{0.5 \cdot \rho \cdot (U_1 - U_2)^2}$$

P_2 was the averaged pressure measured at the wall in the inlet section of the low speed flow. P_v was the vapor pressure which depends on the water temperature.

Downstream of the water pump the flow was divided in two separated flows: in the following study, the high speed one is reference with index 1 and the low speed one index 2. Then both flows crossed a settling chamber containing honeycomb frames and grids in order to homogenize the flow and to break large scale structures. Further on, flows were accelerated in convergent pipes: boundary layers were reduced to restrict the wake effect at the splitting plate tip. Based on the method described in [10], convergent profiles has been optimized to avoid flow separation and cavitation at the wall.

Two different cases were studied:

- case 1, called CDM, was a traditional mixing layer. The inlet conditions were U_1 = 15.8 m/s for the high speed layer and U_2= 3.5 m/s for the low speed layer (figure 1).
- case 2, called MD, was a downward facing step. The inlet conditions were U_1 = 13.5 m/s for the high speed layer and U_2 is null.

For each case, five operating points were selected: one without cavitation (*noncav*), one at the inception (*cav0*) and three with developed cavitating structures (*cav1* to *cav3*). The corresponding cavitation numbers are presented in table 1.

Case		σ_{ref}
CDM	Cav0	0.208
CDM	Cav1	0.167
CDM	Cav2	0.102
CDM	Cav3	0.012
MD	Cav0	0.258
MD	Cav1	0.132
MD	Cav2	0.121
MD	Cav3	0.086

Table 1. operating points.

Temperature measurement of the water was required to calculate the vapor pressure and to set the selected cavitation number. The recorded water temperature varied within the range of 10°C to 25°C depending on operating and atmospheric conditions.

The concentration of dissolved gas inside the water plays a major role in cavitation inception [9]. The experimental apparatus allowed us to measure but not to control the concentration of dissolved gas. The concentration of dissolved O_2 was acquired with an Orbisphere MOCA O2 probe. A degasification protocol has been established in order to reach a minimum value of 3.5 ppm used for each operating point.

Particle Image Velocimetry (PIV)

Velocity measurement was performed in the longitudinal section (X-Y). We were then using 2D PIV-LIF technique in order to obtain the mean and fluctuating components of the velocity field inside the two phase part of the mixing layer. The PIV-LIF system was a LaVision DAVIS with a Twins Ultra Yag 2*30mJ Laser, wave length peak at 532 nm. An Imager ProX2M camera with a minimum interframe time of 110 ns was used to record the PIV-LIF images.

The aim being to measure velocity of the liquid, different couples of filter/particle have been tested in order to vanish the bubbles and highlight the particles which were carried along within the liquid. The selected filter was a high-pass band at 570 nm and the corresponding particles were Rhodamine B type: it absorbs 532 nm light and emits at 584 nm.

A test pattern has been used to focus the devices on the middle vertical plan.

5000 pairs of picture have been recorded by the acquisition system. The delay between the two pictures was 120µs. DaVis 7.2 software was used to cross-correlate the pictures and gave instantaneous velocity field for each pair of pictures. A velocity vector was defined on each node of a 1.38 mm square mesh. The measurement area was 232 mm long and 71 mm high (Fig. 3).

The statistical convergence of velocity measurement has been studied over the whole measurement area: it showed that a minimum of 500 velocity vectors are needed to define the averaged velocity within a precision of ± 0.1 m/s and the standard deviation within ± 0.3 m/s. The Skewness and the flatness factors did not converge with 5000 values of instantaneous velocity therefore those two parameters cannot be analyzed in the present study.

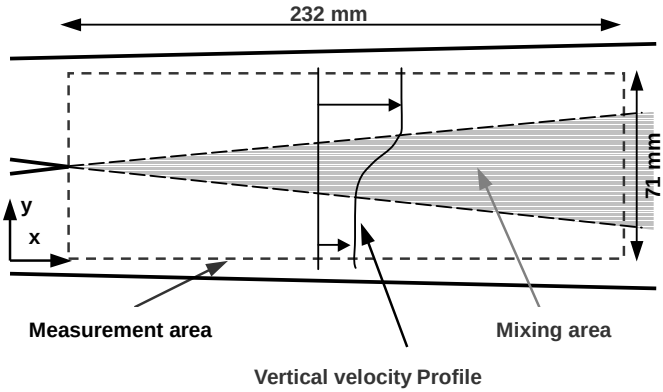

Figure 3. Localization of the measurement area

Dimensionless parameters

The aim was to analyze the self-similarity of the flow from velocity field measurements. Averaged velocity and fluctuations were considered. All parameters were dimensionless in order to be compared to the ones found in the literature about either compressible or incompressible fluid, two-phase or one-phase flows.

The studied parameters are the following:

- vorticity thickness: δ_w [m]
- growth rate: $\delta_w' = \frac{d\delta_w}{dx}$
- y-axis: $y^* = \frac{y - y_{ref}}{\delta_w}$ where y_{ref} is the center of the mixing area.

The splitting plate tip is located at x = 0 and y = 0.

The location Y* = ±1 corresponds to the border of the mixing area.

- velocity gradient (averaged): $\Delta U = U_1 - U_2$ [m/s]
- averaged velocity: $\overline{U}$ and $\overline{V}$ [m/s]
- dimensionless velocity (averaged): $U^* = \frac{U - U_2}{\Delta U}$
- n : number of measurements
- instantaneous velocity: U_i and V_i [m/s]
- longitudinal fluctuations:

$$u' = \sqrt{\frac{\sum_{i=1}^{n} \left(U_i - \overline{U}\right)^2}{n}} \text{ [m/s]}; \quad u'^* = \frac{u'}{\Delta U}$$

- transverse fluctuations:

$$v' = \sqrt{\frac{\sum_{i=1}^{n} \left(V_i - \overline{V}\right)^2}{n}} \text{ [m/s]}; \quad v'^* = \frac{v'}{\Delta U}$$

- turbulent diffusion:

$$u'v' = \frac{\sum_{i=1}^{n} \left(U_i - \overline{U}\right)\left(V_i - \overline{V}\right)}{n} \text{ [m²/s²]}; \quad u'v'^* = \frac{u'v'}{\Delta U^2}$$

- Cinematic Reynolds stress tensor: $\begin{bmatrix} u'^2 & u'v' \\ u'v' & v'^2 \end{bmatrix}$ [m²/s²]

$$R_{ij} = 2k\left[b_{ij} + \tfrac{1}{3}\delta_{ij}\right]$$

- turbulent kinetic energy: $k = \frac{u'^2 + v'^2 + w'^2}{2}$ [m²/s²]
- anisotropy tensor: $b_{ij} = \frac{u'_i u'_j}{2k} - \frac{1}{3}\delta_{ij}$

where: $u'_1 = u'$, $u'_2 = v'$, $u'_3 = w'$

RESULTS AND DISCUSSION

Averaged longitudinal velocity

Fig.4 and Fig.5 were extracted from DaVis 7.2 software, they present the averaged longitudinal velocity U over the entire measurement area. At the operating point CDM (Fig.4) the expansion of the mixing area could be observed (from left to right): this is the area where the velocity varies from U_2 to U_1.

Figure 4. CDM - Cav3- Averaged velocity U.

The MD configuration flow showed a large recirculating area where U is negative (darkest gray area in Fig.5). This area extended further downstream the measurement area at low σ_{ref} (*noncav* Fig.5 and *cav0* Fig.6). Two vortices with opposite vorticity directions were observed.

As a first qualitative observation, we noticed a change of behavior in the evolution of the recirculation area depending on σ_{ref} . The downstream limit of this area is the reattachment point of the flow located on the bottom wall. This point is circled in the Fig.6 to Fig.9. Its location changed depending on σ_{ref} : From no cavitation to low cavitation (from *noncav* Fig.5, to *cav1* Fig.7) the recirculating area decreased. Then the behavior changed: for lower σ_{ref} the recirculating area grew back (Fig.7. to Fig.9).

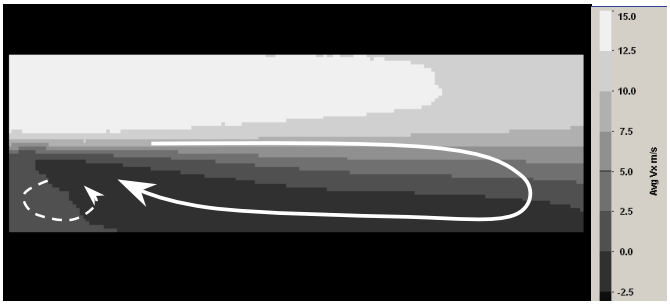

Figure 5. MD – noncav - Averaged velocity U.

Figure 6. MD – cav0 - U

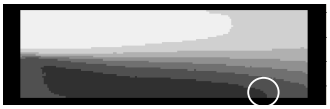

Figure 7. MD – cav1 – U

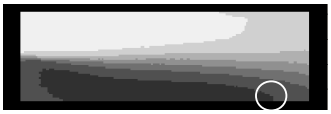

Figure 8. MD – cav2 - U

Figure 9. MD – cav3 – U

From the averaged velocity fields, vertical velocity profiles could be investigated. In order to qualify the mixing area and to analyze its self-similar behavior, 20 vertical profiles have been analyzed: X2 to X21, with a 11 mm distance from each other along the x-axis.

Dimensionless velocity profiles have been plotted and superimposed separately for each studied operating point. As examples, Fig.10 and Fig.11 present Y*(U*) at CDM and MD configurations case *cav3*.

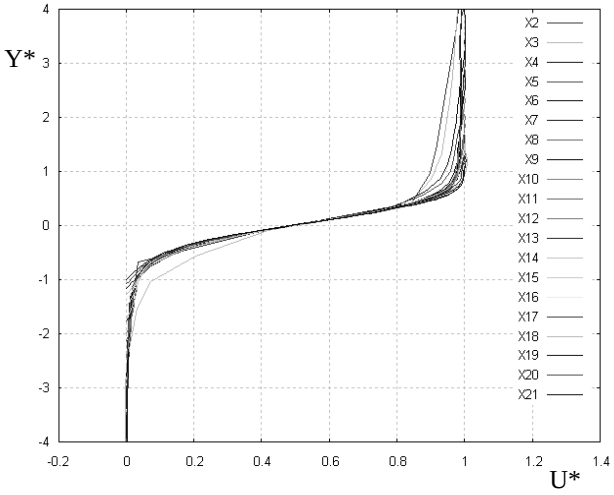

Figure 10. CDM – cav3 - Y(U*)*

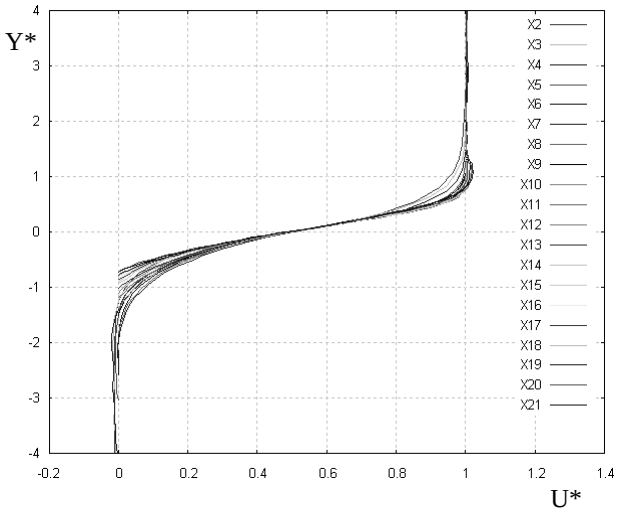

Figure 11. MD – cav3 - Y(U*)*

In the CDM case, Fig.10, at the upper border of the mixing layer (Y* = 1), we observed smaller velocities at X2 to X8 than on the other profiles. This phenomenon was due to a flow separation and wake effect on the splitting plate tip. This problem influenced the mixing area in the CDM configuration until X8, further, the profiles were well superimposed and the behavior was self-similar. No major changes depending on σ_{ref} were observed.

In the MD case, the influence of the splitting plate tip was noticed until X6. Another change of behavior was observed: the maximum velocity of the downstream profiles was higher than U_1 (U* = 1) and located at Y* = 1 (From X15). This phenomenon was amplified as σ_{ref} decreased; it was probably linked to the dynamic behavior of the reattachment area with a pressure gradient from downstream. The shear layer was curved: Y_{ref} decreased along x-axis. According to the observations, only a minor part of the mixing area could be approximated self similar: from X7 to X14.

Vorticity thickness and growth rate

The vorticity thickness characterizes the development of the Kelvin-Helmholtz instabilities at the interface of the layers. δ_w grows linearly along x-axis when the flow is self-similar:

$$\delta_w' = \frac{d\delta_w}{dx} = \text{constant}$$

From the velocity profiles, it was possible to define $\delta_w(x)$ which is plotted in Fig.12 and Fig.13 for each operating point. The dotted lines mark the boundary of the self-similar area presented in the previous subsection.

δ_w' is a function of fluid properties and inlet conditions [8]:

$\delta_w' = \delta_w'(r,s)$ (for incompressible fluid)

where $r = U_2/U_1$ and $s = \rho_2/\rho_1$

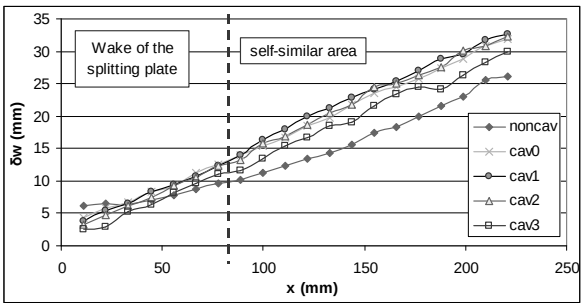

Figure 12. CDM – $\delta_w(x)$ – Vorticity thickness

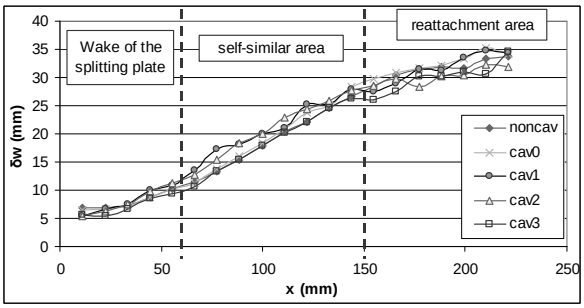

Figure 13. MD – $\delta_w(x)$ – Vorticity thickness

In the present study, both layers were liquid water and therefore $\rho_2/\rho_1=1$ and $s=1$. δ_w' was reduced to:

$$\delta_w'=C\frac{1+r}{1-r}$$

where C is a constant defined experimentally with a downward facing step flow where r = 0 and therefore $\delta_w'=C$.

Dimotakis (1986) [11] defined C in the range of 0.16 to 0.18. Brown and Roshko (1974) [8] recommend C = 0.181. The results were compared to this reference for each studied cases (Fig.14). According to the literature, experimental values vary within ±20% around those references for all the incompressible flows tested. Referring to compressible flows, with equivalent s and r, vorticity thickness could be five times smaller [7-8].

Fig.14 presents the ratio of δ_w' on the consensus $\left(C\frac{1+r}{1-r}\right)$. We noticed that the operating point without cavitation, CDM and MD cases *noncav*, followed Brown and Roshko (1974) [8] results within less than 10% difference. Regarding to the cavitating cases, results were also included in the range of values presented in the literature concerning incompressible flows.

Analyzing these first results, we may concluded that development of cavitating structures did not strongly influence the global development of the vortices. However, in the CDM configuration, vorticity thickness seemed bigger, about 30% more in the cavitating cases than in the non cavitating one even if the corresponding growth rates were similar in the downstream part of the flow. This difference in final thickness is due to the fact that, at the beginning of the shear layer expansion (for x ranging from 50 to 150mm), the non cavitating flow (in the CDM case) has not reached its asymptotic growth rate. At the opposite, cavitating configurations seems to attain more rapidly their autosimilar state.

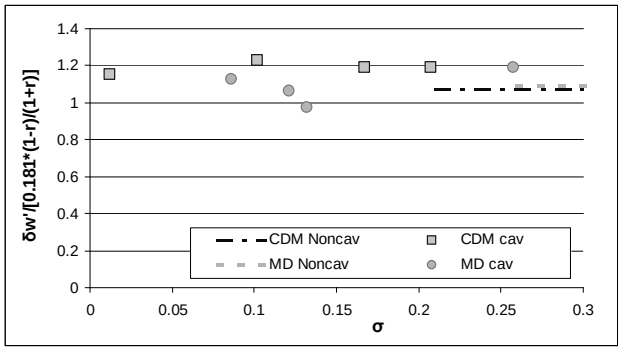

Figure 14. Growth rate comparison

Turbulent shear flow

Fluctuations of the velocity field have been analyzed. Fig.15 presents as an example the longitudinal fluctuations u'* in the case CDM *noncav* where vertical profiles have been superimposed along x-axis (from X2 to X21). Transversal fluctuations and turbulent diffusion profiles had similar shapes: The first common point was a very low and constant value outside the mixing area (Y* > 1 and Y* < -1) and the second was a maximum value reached at the center of the mixing area (Y* = 0).

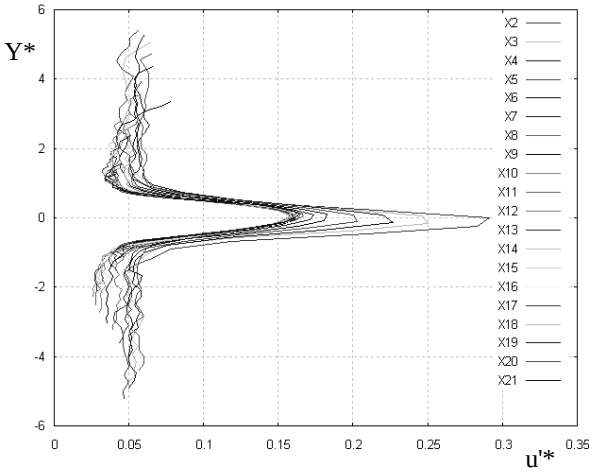

Figure 15. CDM – noncav - longitudinal velocity fluctuations

In a self similar shear flow, fluctuation profiles are superimposed, the maximum value is constant along x-axis. From Fig.15 we observed that the maximum of the profiles in the wake of the splitting plate differed from the ones downstream: The longitudinal fluctuations were not self similar from X2 to X7 in that case.

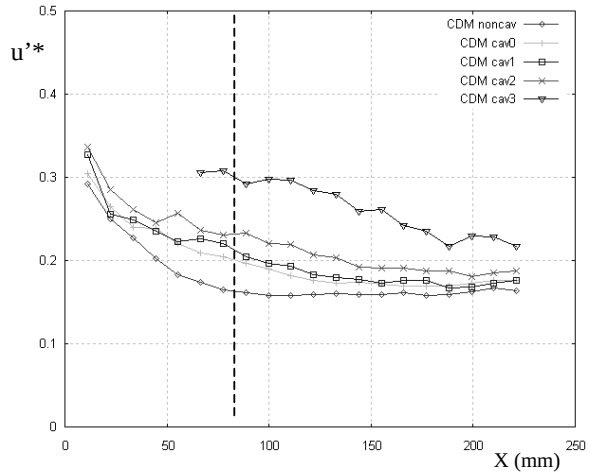

Figure 16. CDM – Maximum longitudinal velocity fluctuations

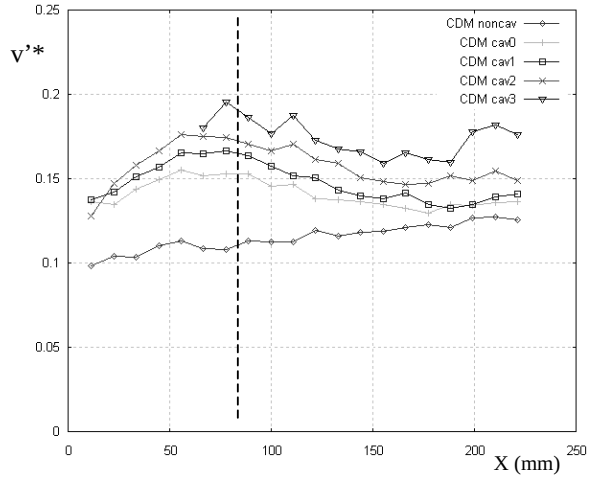

Figure 17. CDM – Maximum transverse velocity fluctuations

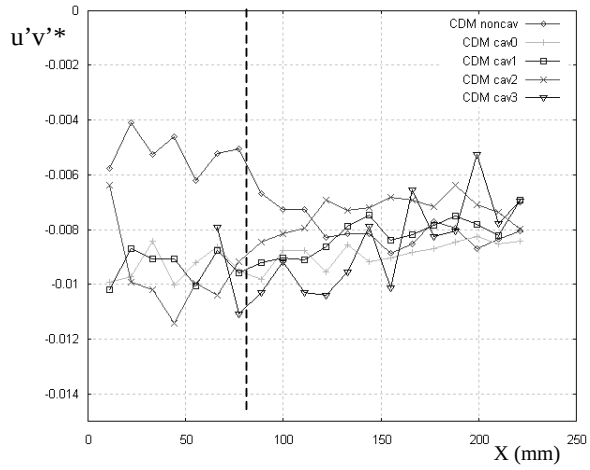

Figure 18. CDM – Maximum turbulent diffusion

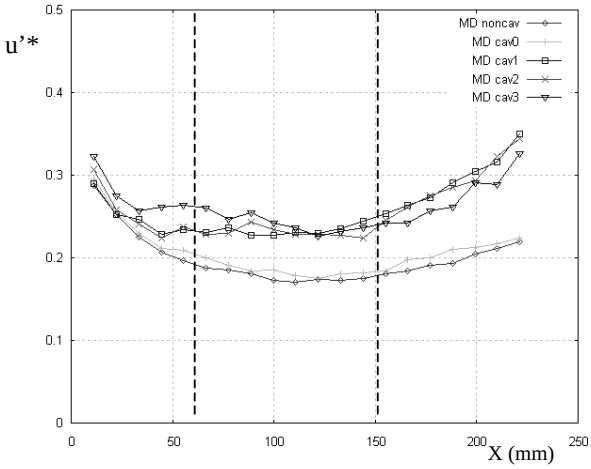

Figure 19. MD – Maximum longitudinal velocity fluctuations

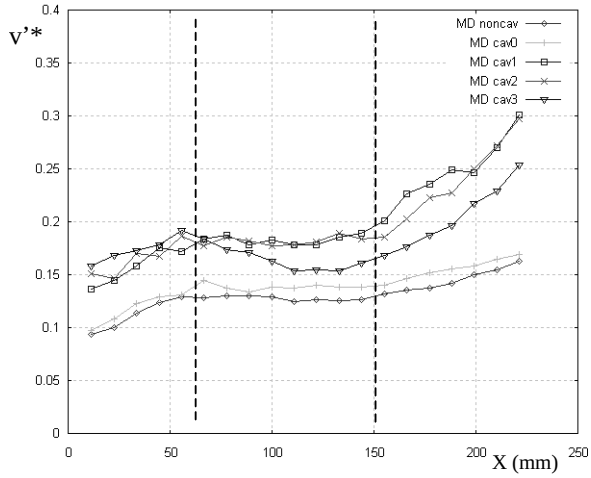

Figure 20. MD – Maximum transverse velocity fluctuations

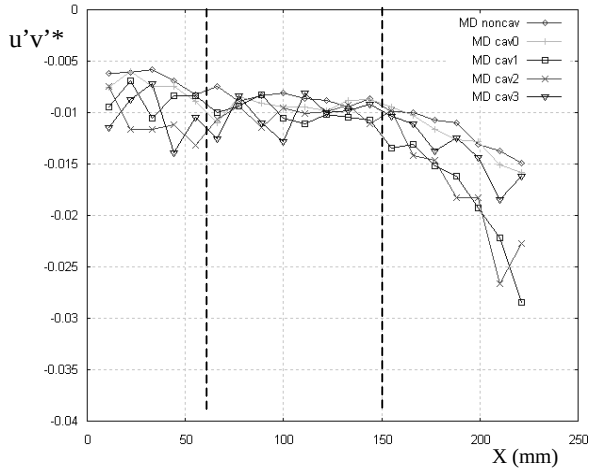

Figure 21. MD – Maximum turbulent diffusion

Evolution along x-axis of the maximum of those profiles has been studied for each operating point. Results are presented in Fig.16 to Fig.21. The dotted lines mark the boundary of the self-similar area presented in previous subsections. Those borders, based on mean velocity analysis, corresponded to the zone where the maximum of the fluctuation profiles seemed to be constant (Fig.16 to Fig.21). This confirmed the localization of the self similar part of the flows.

In the CDM case, u'* and v'* increased when cavitation developed (Fig.16 and Fig.17). In the downward facing step case (MD, Fig.19, Fig.20 Fig.21), the fluctuations u'*, v'* and u'v'* showed a strong growth around the reattachment area, X15 to 21. This tendency corresponded to an unsteady behavior: the recirculating area was probably pulsating and vortices were certainly convected downstream. Further study will characterize the frequencies of the instabilities.

In the MD case (Fig.20), the transversal fluctuation v'* clearly showed a behavior change similar to the evolution of the reattachment point (see Fig.5 to Fig.9): when σ_{ref} decreased, v'* grew until $\sigma_{ref} = 0.13$ then v'* decreased. Longitudinal fluctuations did not show a behavior change, u'* grew as σ_{ref} decreased. This highlighted strong transversal instabilities depending on the dynamic of the recirculation area.

The turbulent diffusion u'v'* was null outside the mixing area (Y* > 1 or Y* < -1), this mean that there is no correlation between longitudinal and transversal fluctuations. This was typical of an isotropic homogeneous turbulence behavior.

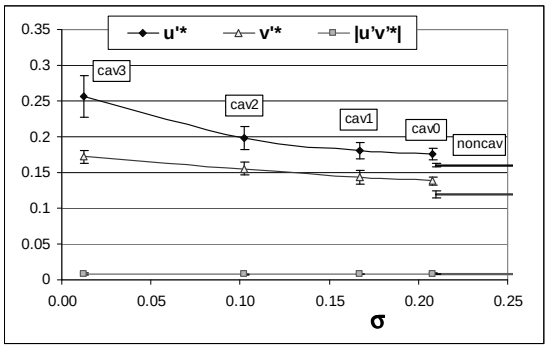

Figure 22. CDM – fluctuations in the self-similar area

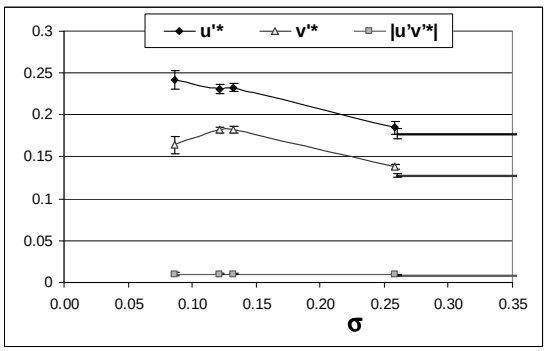

Figure 23. MD – fluctuations in the self-similar area

Fig.22 and Fig.23 bring together the main results concerning the turbulence properties of the mixing area in both cases: CDM and MD for each operation point. Average values and spatial standard deviations of u'*, v'* and u'v'* were plotted. They were defined by only taking into account the values inside the self similar area. As an example, in the MD cases u'* was defined:

$$\overline{u'^*} = \frac{\sum_{i=7}^{14} u'^*(Xi)}{8}$$

and its standard deviation: $$\sigma_{u'^*} = \sqrt{\frac{\sum_{i=7}^{14} \left(u'^*(Xi) - \overline{u'^*}\right)^2}{8}}$$

Longitudinal fluctuations had bigger amplitude than the transversal ones (Fig.22 and Fig.23), this tendency is observed as well in every typical flows like shear flow, boundary layer or wake flow.

From results presented Fig.22 and Fig.23 we concluded that there was no evolution of u'v'* when cavitation developed. u'* and v'* increased respectively by 60% and 44% in the CDM case comparing the working point without cavitation (*noncav*) and the most cavitating (*cav3*) one. In the MD cases, they increased respectively by 36% and 29%.

From those results, evolution of Reynolds tensor components was defined over the studied σ_{ref} range. It will be used as reference to validate turbulence models in numerical simulations.

We noticed a difference in the evolution of those parameters by comparing the CDM and MD cases. Concerning CDM, u'* and v'* grew as σ_{ref} decreased whereas in the MD case a quasi saturation of the turbulence level occurred from $\sigma_{ref} = 0.13$. Consequently, from this point ($\sigma_{ref} = 0.13$), the flow seemed to be ruled by the reattachment dynamic and the cavitation-turbulence relation seemed to be fixed.

Turbulent kinetic energy

The kinetic energy is the sum of the three components u'², v'² and w'². The third one concerns fluctuations of the third component of the velocity, W, which was not measured during this PIV-LIF campaign. Wygnanski et al. (1970) [12] measured w' in a downward facing step (flow without cavitation). w' has been compared to u' : w'/u' = 0.85. This was the ratio we used to estimate the missing component of the kinetic energy k for the present paper. Fig.24 and 25 shows the evolution of the maximum of the turbulent kinetic energy when the overall cavitation level is increased (by decreasing σ_{ref}) for CDM and MD cases respectively

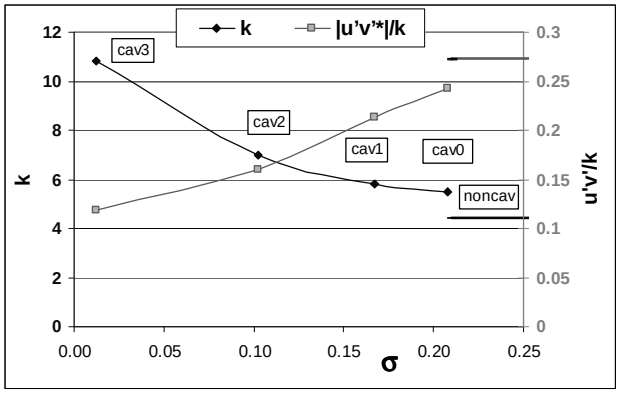

Figure 24. CDM – kinetic energy in the self-similar area

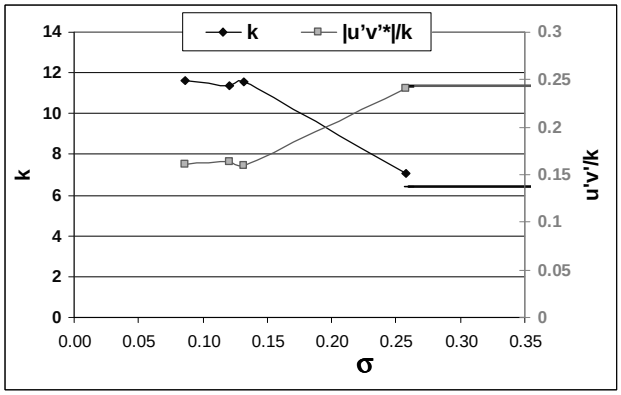

Figure 25. MD – kinetic energy in the self-similar area

The kinetic energy has doubled between the flow without cavitation and the most cavitating one in both configurations (CDM and MD). The shear rate being constant over the range of σ_{ref} studied, the growth of kinetic energy came from the vaporization and implosion of the cavitating bubbles.

In MD case, according to the behavior of u' and v', k grew until $\sigma_{ref} = 0.13$ and then stayed constant.

In Fig.24 and Fig.25 the parameter $\frac{|u'v'|}{k}$ is also plotted for each studied σ_{ref}. This parameter is used as a reducer factor in numerical models: Bradshaw 's hypothesis applied to one-phase 2D flows gave: $\frac{|u'v'|}{k} \leq 0.3$

We noticed that the Bradshaw's hypothesis is verified in the presented experiment for all operating points, cavitating or not.

In CDM case, $\frac{|u'v'|}{k}$ decreased significantly and continuously when cavitation developed (we observed a coefficient 2 between *noncav* and *cav3)*. Thus the turbulence production level represented by u'v' was more efficiently converted to turbulent kinetic energy when cavitation was strongly developed. Successive vaporizations and condensations of the fluid particles inside the turbulent area have generated additional velocity fluctuations due to strong density changes.

Anisotropy tensor

Evolutions of the four main terms of the anisotropy tensor for each working point were analyzed (CDM case Fig.26 and MD case Fig.27). b_{11} and b_{33} were linked because w' fluctuations were deduced from u' using a constant factor (w'/u' = 0.85).

In CDM cases, when σ_{ref} decreased, the longitudinal part of the fluctuations contained in the global turbulent kinetic energy k increased significantly from $\sigma_{ref} = 0.10$ (*cav2*). The growth from u' (b_{11}) was followed by a decrease of v' (b_{22}). In addition, the growth of b_{12} was steady all over the studied σ_{ref} range.

We observed therefore a major change in the evolution of anisotropy between *cav2* and *cav3* cases (Fig.26). However, the ratio between the turbulent shear rate and the turbulent kinetic energy (b_{12}) grew continuously principally due to the constant raise of k because as we have seen, the turbulent shear (u'v') was quasi-constant over the σ_{ref} studied range. As a result, Reynolds tensor was modified as cavitation developed and especially from *cav2*. It seemed that cavitation increased turbulent fluctuation rate without affecting turbulent shearing rate and probably without modifying the turbulent viscosity. In addition, when cavitation was strongly developed, a significant change in the anisotropy of Reynolds tensor was noticed in which longitudinal fluctuations were advantaged compare to the transverse ones.

In the MD cases (Fig.27), we observed tendencies similar to the CDM cases except for the b_{12} term which stabilized from *cav1* because k stopped growing at that point. In this configuration, the turbulent field underwent external stresses (reattachment of the flow, large scale unsteadiness, longitudinal pressure gradient) and so k tended to saturate. Nevertheless, at low σ_{ref}, values of b_{11} grew while b_{22} decreased.

The MD configuration was more complex to analyze and most of all it did not let the turbulence-cavitation coupling free from external constraints. However, it was probably more representative of real complex flows situations.

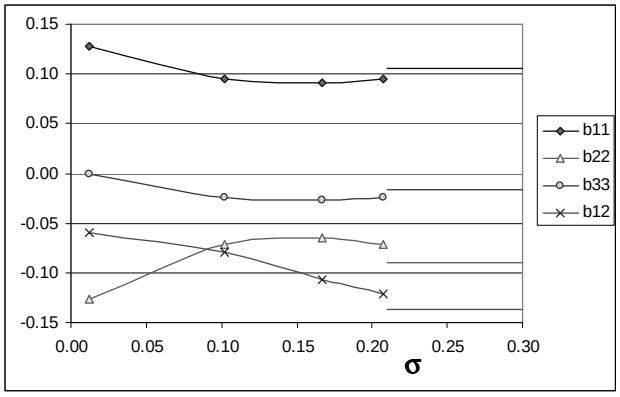

Figure 26. CDM – Anisotropy tensor components

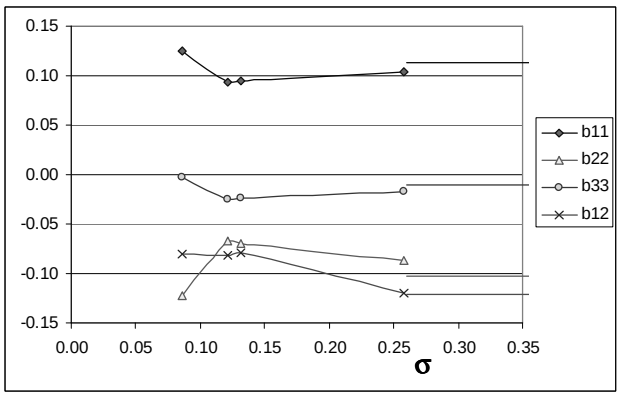

Figure 27. MD – Anisotropy tensor components

CONCLUSION

Velocity measurements were performed with a PIV-LIF system in a 2d cavitating shear layer flow. Acquisition of instantaneous velocity fields allowed us to analyze the dynamic of the flow for two distinct configurations: a mixing layer flow (CDM) and a downward facing step flow (MD).

Averages and fluctuations values have been validated by analyzing the convergence of the measurements.

The dimensionless analysis of mean velocity profiles and fluctuations profiles led us to localize the self similar area. Parameters that characterized the flow dynamic were studied and quantified: Vorticity thickness, growth rate and Reynolds tensor components. Turbulent kinetic energy and the anisotropy tensor components were also analyzed and estimated. Those parameters will be used as references for validation of turbulence models in numerical simulations.

General behaviors of the two configurations have been observed:

- In the CDM cases, the mixing area developed a turbulent shear area along the x-axis, growing linearly, showing a constant growth rate over the studied cavitation levels (range of σ_{ref}). The flow seemed isobaric in the external layers.

- MD cases were more complex, presenting flow separation with a large recirculating area and a pressure gradient from downstream. The reattachment point moved depending on σ_{ref} , its evolution was not a bijection. The flow seemed to have an unsteady behavior and was certainly pulsing and shedding vortices downstream.

The main results of this study clearly showed that the turbulence-cavitation relationship inside a mixing layer was not a simple change of compressibility properties of the fluid in the turbulent field due to the existence of a two-phase flow. We observed quite different phenomena as compared to the one observed in one-phase compressible flows so physical properties of one-phase supersonic flows could not be used as they are.

The presented results will be implemented with void ratio measurements. This will provide information concerning the momentum: ρU profiles inside the mixing area will be analyzed in order to provide a better understanding of the physical properties and dynamic of such cavitating flows.

ACKNOWLEDGMENTS

The authors wish to express their gratitude to the French Space Agency (CNES) and the rocket engine division of SNECMA for their continuous support. Fruitful collaboration with S. Prothin (Ecole Navale) and H. Djeridi (Brest University) and strong technical support by L. Vignal (LEGI, Grenoble) are also greatly acknowledged.

REFERENCES

[1] Barre S., Rolland J., Boitel G., Goncalves E., Fortes-Patella R. (2008), Experiments and modelling of cavitating flows in venturi: attached sheet cavitation, European Journal of Mechanics/Bfluids (in press)

[2] Rolland J., Boitel G., Barre S.,Fortes Patella R. (2006), Experiments and modelling of cavitating flows in Venturi, Part I: stable cavitation, Sixth Internationnal Symposium on Cavitation, CAV2006, Wageningen, the Netherlands, September 2006.

[3] Fortes Patella R., Barre S., Reboud J.L., (2006), Experiments and modelling of cavitating flows in Venturi, Part II: unsteady cavitation, Sixth Internationnal Symposium on Cavitation, CAV2006, Wageningen, the Netherlands, September 2006.

[4] Merle L. (1994) Etude expérimentale et modèle physique d'un écoulement cavitant avec effet thermodynamique, Ph.D. Thesis, Grenoble Institue of Technology.

[5] Stutz, B., Reboud, JL (1997), Two-phase flow structure of sheet cavitation, Phys. Fluids 9(12).

[6] Stutz, B., Reboud, JL (2000), Measurements within unsteady cavitation, Experiments in Fluids,n°29, pp545-552.

[7] Papamoschou, D., Roshko, A. (1988), The compressible turbulent shear layer: an experimental study, Journal of Fluid Mechanics, vol.197, pp.453-477

[8] Brown, G., Roshko, A. (1974), On density effects and large structure in turbulent mixing layers, Journal of Fluid Mechanics, vol.64, part 4, pp.775-816
[9] Arndt, R.E.A. (2002), Cavitation in Vortical Flows, Annu. Rev. Fluid Mech., vol. 34, pp. 145-175
[10] Sargison, J.E., Walter, G.J., Rossi, R (2004), Design and calibration of a wind tunnel with a two dimensional contraction, 15th Australian Fluid Mechanics Conference, Sydney, Australia, 13-17 Dec
[11] Dimotakis, P.E. (1986), Two dimensional shear-layer entrainment, AIAA J., vol. 24 (11), pp. 1791-1796.
[12] Wygnanski, I., Fiedler, H.E. (1970), The two-dimensional mixing region, J. Fluid Mech., vol. 41, part 2, pp. 327-361.